Structural and magnetic properties of the ternary solid solution between CoSb and $Fe_{1+\delta}Sb$

P. Amornpitoksuk,[1] D. Ravot,[1] A. Mauger,[2] and J. C. Tedenac[1]
[1]*Institut Charles Gerhardt, CNRS, UMR 5253,* Université de Montpellier 2, Place Eugène Bataillon, 34095 Montpellier Cedex 5, France*
[2]*Institut de Minéralogie et Physique des Milieux Condensés, Université Paris 6, 140 rue de Lourmel, 75015 Paris, France*
(Received 19 October 2007; revised manuscript received 7 January 2008; published 3 April 2008)

The ternary solid solution relating CoSb and $Fe_{1+\delta}Sb$ has been synthesized and the Fe spin dilution effects on the magnetic properties has been investigated. The Fe magnetic moments are localized despite the fact that the metallic character increases with the Fe concentration. The covalent bonding along the *c* direction that is responsible for the metallic character is also responsible for a smaller magnetic moment on Fe sites, which depends on the Fe concentration. On the Fe-rich side, the antiferromagnetic (AF) ordering is observed down to a Fe concentration that is comparable to the site percolation threshold for the basal plane. At lower temperatures, re-entrant spin-glass phases are observed, which become spin-glass phases below the percolation threshold for AF ordering. The dynamic scaling shows the same behavior as that of the conventional spin glasses in which the Ising anisotropy is small.

DOI: 10.1103/PhysRevB.77.144405 PACS number(s): 75.20.−g, 75.50.Pp

I. INTRODUCTION

T_rX samples, where T_r is a transition metal and X is a metalloid, form a large variety of materials that crystallize in the NiAs structure. Primary applications of such materials concern ferromagnetic compounds, such as MnSb and MnBi.[1] Transition metal antimonides of the family, however, are not all ferromagnetic.[1] FeSb is antiferromagnetic[1] and CoSb is paramagnetic. In this framework, we found that it is desirable to study the magnetic properties of materials relating CoSb and FeSb, completing the investigation of the Co-Sb-Te ternary system.[2]

The NiAs structure illustrated in Fig. 1 can be viewed as hcp and as a sublattice with Ni atoms in the octahedral interstices, while tetrahedral interstices are vacant. The substitution of Co by Fe atoms on the (2*a*) Wickoff sites is accompanied with a partial population of the (2*d*) interstitial sites by Fe. As a consequence, FeSb is always nonstoichiometric and its actual chemical composition is $Fe_{1+\delta}Sb$ with $\delta \geqslant 0.02$. On the other hand, this deviation from stoichiometry allows the solid solution to retain the NiAs structure upon substitution of Co by Fe in the whole range of concentrations [Fe] and [Co] of the metal ions in the ratio $0 \leqslant [Fe]/([Fe]+[Co]) \leqslant 1$.

The broad variety in magnetic behaviors present in T_rX materials comes from the fact that the bonding is a combination of ionic and unsaturated covalent (metallic) characters in proportion that depends on the choice of the transition element and the metalloid. The c/a ratio is important to have an indirect insight on the ionic or metallic character of the material. Phases with large c/a ratios tend to be ionic, such as the case of NiS, which realizes the exact close-packing hexagonal ratio $c/a=1.633$. Phases with smaller c/a are more metallic (e.g., NiAs with $c/a=1.39$). For this reason, the x-ray diffraction (XRD) analysis has been performed on our samples not only as a means of characterization but also to determine the evolution of the c/a ratios along the series. As a result, CoSb has a partly metallic character and $Fe_{1.27}Sb$ is even more metallic than CoSb.

Many works have been devoted to magnetic properties of $Fe_{1+\delta}Sb$, but the results are divergent. Yashiro *et al.*[3] reported a transition to the antiferromagnetic ordering of the magnetic moments on (2*a*) iron sites at the Néel temperature $T_N=105$ K for $\delta=0.14$, while the ordering of the magnetic moments on the Fe (2*d*) interstitial sites takes place only at $T_{ni}=25$ K. On the other hand, Kumar *et al.*[4] reported that the Fe interstitials ordered also at T_N. However, powder neutron diffraction did not evidence any spin freezing of the Fe-interstitial moments down to 10 K.[3] Nössel and Sondermann concluded that the interstitial Fe atoms order indeed at 10 K,[5] whereas other authors concluded that these form magnetic micromagnets near 28 K.[6] In view of these divergent results, we found that it is necessary to pursue the investigation of the magnetic properties of these materials.

The paper is organized as follows. Section II is devoted to the preparation of the materials, and their structural properties are reported in Sec. III. The magnetic properties in the paramagnetic phase are the subject of Sec. IV, in which the link with the electronic structure is also discussed. The mag-

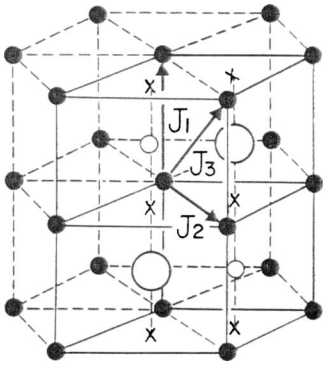

FIG. 1. Picture of the crystal structure of CoSb from Ref. 3 The Co atoms are represented by full circles. The sites occupied by Sb are the larger open circles. The smaller open circles represent the (2*d*) sites that are not occupied in CoSb but partly occupied by iron in the $Co_yFe_xSb_z$ samples investigated in this work. $J_{1,2,3}$ refer to the magnetic interactions mentioned in the text.

TABLE I. Sample composition and effective magnetic moment deduced from the Curie–Weiss law. The magnetic moment at $x=0.50$ could not be determined because of the high Néel temperature ($\simeq$200 K) for this particular sample (see Sec. V in the text).

Sample composition			Moment in μ_B
Co	Fe	Sb	
0.50	$x=0$	0.50	
0.495	$x=0.01$	0.495	
0.48	$x=0.03$	0.49	
0.465	$x=0.05$	0.485	1.62
0.40	$x=0.12$	0.48	2.25
0.33	$x=0.20$	0.47	2.72
0.24	$x=0.30$	0.46	3.45
0.15	$x=0.40$	0.45	3.54
0.06	$x=0.50$	0.44	
0	$x=0.56$	0.44	3.67

netic freezing is investigated in Sec. V. The Fe-rich samples show a transition to antiferromagnetic order. For lower Fe concentrations, we find re-entrant spin-glass phases that become spin-glass phases below the percolation threshold for the onset of long-range antiferromagnetic ordering. The results are discussed in Sec. VI.

II. EXPERIMENT

Synthesis of the samples takes place in two steps. First, the required amounts of the elements (high purity grade, >99.99%) Sb, Co, and Fe are introduced in a quartz tube (inner diameter: 0.8 cm) in a glove box under argon atmosphere. After sealing under vacuum (residual pressure lower than 10^{-5} torr), the charge was heated at 1100 °C for one week and then quenched into water. Second, the samples are annealed at 900 °C for one week. To avoid the breaking of the quartz tube due to the large expansion of the (Co, Fe)Sb compounds during this annealing process, samples are transferred in a larger tube (inner diameter: 1 cm) before the annealing at 900 °C. This temperature was chosen because it is smaller than the eutectic temperature in binary Co-Sb (1065 °C) (Ref. 7) and Fe-Sb (996 °C).[8]

The composition of the samples was determined by using a scanning electron microscope. For this purpose, the samples were embedded in epoxy resin and polished down to a 1 μm diamond grade paste. These samples were then coated with a thin layer of graphitic carbon to obtain a good electric sheet conductivity. The composition was analyzed with a Cambridge electron probe by using energy-dispersive x-ray spectroscopy and wavelength dispersion x-ray spectroscopy (WDS). In particular, the concentration profile for Co, Fe, and Sb was detected by the WDS line scan method. The line scans were flat, so the samples were homogeneous. The final compositions were found to be in agreement with the initial compositions determined by the relative concentrations of the precursors (Table I).

Due to the deviation of stoichiometry upon substitution of Co by Fe, the concentration of each element has to be determined to identify the samples. There are several possibilities to write the chemical composition of the samples. One possibility would be to extend the conventional notation $Fe_{1+\delta}Sb$ to write the samples under the form Co_yFe_xSb. However, there is actually no particular reason to choose Sb as the reference component and, instead, we have chosen to report the concentrations under the form $Co_yFe_xSb_z$ with $x+y+z=1$, and we shall refer to the samples by their corresponding x value in the text. For instance, the sample $Fe_{1.27}Sb$ is now written as $Fe_{0.56}Sb_{0.48}$ (sample $x=0.56$) and CoSb is $Co_{0.50}Sb_{0.50}$ (sample $x=0$). The variable $r=[Fe]/([Fe]+[Co])=x/(x+y)$ that does not depend on the choice to write the composition would be the single pertinent variable if it was the rate of substitution of Co by Fe. However, we shall see in the next section that this parameter fails to have this meaning because part of the Fe is not in substitution to Co, and we shall also give some evidence in the subsequent sections that iron atoms on both sites give different contributions to the magnetic properties.

After they have been annealed, all the samples were grounded with mortar until a fine powder that has been analyzed by XRD was obtained. The patterns have been obtained by using a Seiffert diffractometer in the θ-2θ Bragg–Brentano geometry. The data have been recorded by using the Cu $K\alpha$ radiation at $I=25$ mA and $K=40$ kV with an angular step $\theta=0.01°$ and time step of 5 s. All the samples are single phased and crystallized in the InAs ($B8$) structure and no impurity phase has been detected.

The magnetization $M(H)$ curves have been measured with the use of a MPPS "Quantum Design" magnetometer for magnetic fields in the range of $0 \leqslant H \leqslant 5$ T. The magnetic susceptibility $\chi(T)$ curves have also been measured with the same apparatus in the temperature range of $4.2 \leqslant T \leqslant 300$ K. Two protocols have been used. According to one of them, a static magnetic field $H=0.1$ T is first applied to the sample at room temperature. Then, the magnetization M is recorded upon decreasing the temperature to obtain the field-cooled (FC) magnetic susceptibility $\chi=M/H$ as a function of T. According to the other protocol, the sample is first cooled at 4.2 K before the application of the static magnetic field $H=0.1$ T. Then, the magnetization M is recorded upon heating to obtain the zero-field-cooled (ZFC) magnetic susceptibility $\chi=M/H$. In all the magnetic experiments, attention has been paid to prevent any pollution by oxygen, and the reproducibility of the results has been checked on all the samples.

The ac magnetic susceptibility has been recorded under an ac magnetic field of amplitude of 0.3 mT in the frequency range of 0.1–800 Hz to investigate spin freezing.

III. X-RAY ANALYSIS

The lattice parameters and the ratio c/a deduced from Rietveld refinement are reported in Figs. 2 and 3, respectively, as a function of the iron concentration. In contrast to the small and decreasing variation of c as a function of the iron concentration, a large increase of a is observed, giving evidence of a radius r_{Fe} of iron larger than the cobalt one r_{Co}.

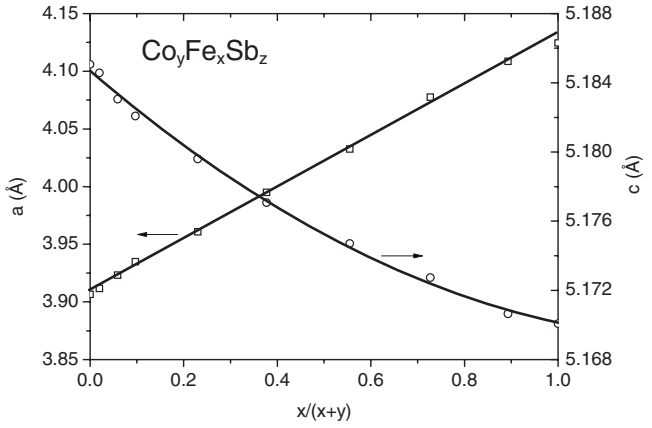

FIG. 2. Variation of the a and c lattice parameters with composition.

Due the small value of the ratio c/a in $Fe_{0.56}Sb_{0.48}$, we can take for granted that this material is metallic so that $r_{Fe} \simeq 1.26$ Å. Note that the metallic radius of Co (1.25 Å) is about the same as that of metallic Fe. Therefore, the smaller radius of Co evidenced by the decrease of a with the Fe concentration implies that r_{Co} is closer to the ionic radius. We shall find in the next section that the cobalt is nonmagnetic, which implies that the ionic valence state should be close to the trivalent state. Indeed, the ionic radius of Co^{3+} is only 0.6 Å. This value, however, is only an estimate because the c/a ratio of $Co_{0.50}Sb_{0.50}$ is small enough to ensure that the ionic limit is not reached in this material. On the other hand, the covalent (metallic) character increases with the [Fe] concentration and the quasisaturation of c/a as [Fe]/([Fe]+[Co]) approaches 1 in Fig. 3 is an evidence that the metallic limit is reached in $Fe_{0.56}Sb_{0.48}$. Note that this saturation of c/a and, hence, the nonlinear variation of this parameter with the Fe concentration are entirely attributable to the nonlinear variation of the parameter c, while the variations of a are linear and satisfy Vegard's law, as can be seen in Fig. 2. This feature can be understood if we note that the basal planes perpendicular to the c axis are occupied by the transition metal elements distributed on a hexagonal lattice of parameter a according to Fig. 1. Therefore, the variation of this parameter a in Fig. 2 is dominated by chemical pressure effects generated by the substitution of transition elements with different radii. This pressure effect is responsible for Vegard's law, which is then satisfied for the parameter a. In $Co_{0.50}Sb_{0.50}$, the space between adjacent Co planes perpendicular to c is occupied only by Sb since the (2d) interstitial sites are empty. The substitution of Co by Fe is accompanied by an increasing occupation rate of these (2d) interstitial sites by Fe. The resulting chemical pressure, however, is negligible because the value of c is mainly determined by the Sb atoms of bigger size (the metallic and covalent radii of Sb are 1.61 and 1.43 Å, respectively). Therefore, the distance c is mainly influenced by the changes in the electrostatic interactions between adjacent Co/Fe atomic planes due to the change in the ionicity of the bonds, so that the variations of c are small and deviate from Vegard's law. This is consistent with the attribution of the decrease of c to an increase of the metallic bonds between neighboring transition metal atoms along the c axis for materials crystallized in this NiAs structure.[9]

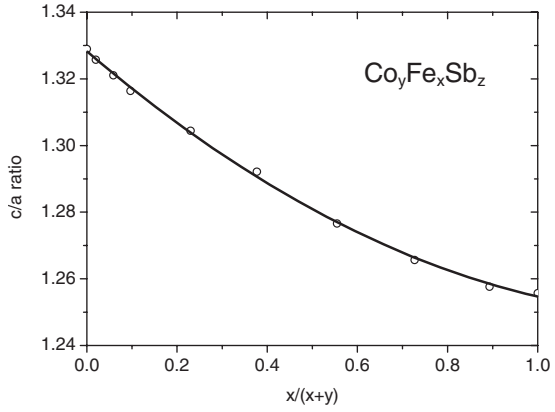

FIG. 3. Evolution of the ratio c/a of the lattice parameters with composition.

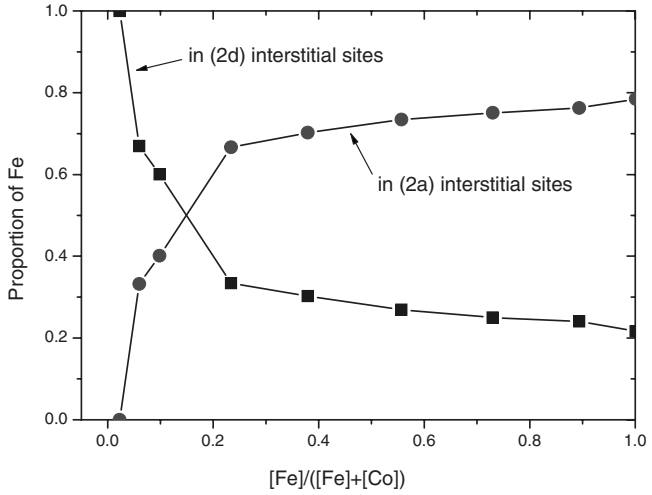

FIG. 4. Repartition of Fe atoms among (2a) and (2d) sites in the samples investigated. The total concentration of Fe is normalized to unity so that the ordinate can be viewed as the probability that a Fe atom occupies a (2a) site (broken curve) or a (2d) site (full curve). Note that the curves are only guides for the eyes; the dots are experimental values.

The difficulty to substitute Co by Fe is evidenced in Table I by the fact that the introduction of 1 at. % of iron in $Co_{0.50}Sb_{0.50}$ gives a sample with chemical composition $Co_{0.495}Sb_{0.495}Fe_{0.01}$, which means that the total amount of Fe occupies (2d) interstitial sites. Only for $x=0.03$ do we have a sample in which a fraction of the iron atoms occupies the (2a) sites (in a concentration of 1 at. % in this particular sample). The proportion of Fe that is in substitution to Co monotonously increases with the [Fe] content x in the matrix, as can be seen in Fig. 4.

IV. MAGNETIC PROPERTIES IN THE PARAMAGNETIC REGIME

A. Experimental results

The magnetic susceptibility curves $\chi(T)$ of the samples with very small Fe concentrations ($x \leqslant 0.03$) are reported in

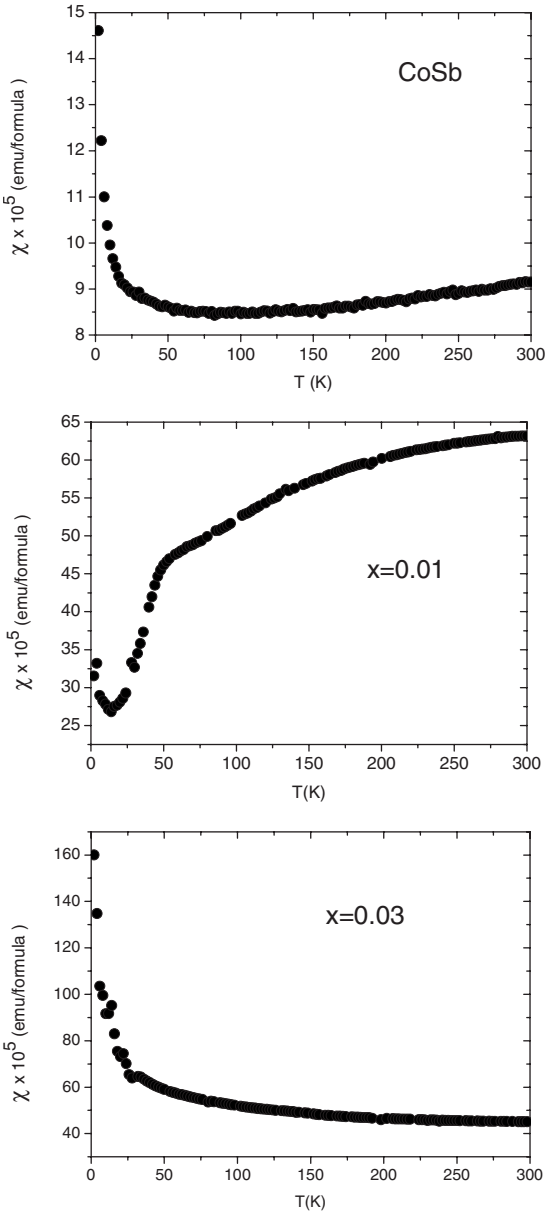

FIG. 5. Magnetic susceptibility $\chi(T)$ measured in dc magnetic field $H=0.1$ T for samples with small Fe concentrations $0 \leqslant x \leqslant 0.03$. No difference between zero-field-cooled and field-cooled protocols defined in the text has been detected for these samples. For $x=0$, the formula is CoSb to make contact with earlier works. For all the $x \neq 0$, the formula is $Co_yFe_xSb_z$ with $x+y+z=1$ (see Table I).

Fig. 5. No difference between FC and ZFC curves can be observed at these small Fe concentrations. The curve $\chi(T)$ of $Co_{0.5}Sb_{0.5}$ is typical of a nonmagnetic metal or semimetal with a Pauli contribution of the free-electron gas in the order of 8×10^{-5} emu per formula, which is almost temperature independent. The increase of χ below 20 K is a $1/T$ contribution of residual impurities that act as uncorrelated spins. The introduction of Fe atoms in the $x=0.01$ sample is responsible for an increase of $\chi(T)$ at room temperature, but this contribution decreases upon cooling, after Fig. 5, presumably due to an antiferromagnetic coupling with the free carriers. In the $x=0.01$ sample, the Fe atoms can then be considered as magnetic impurities located in $(2d)$ sites.

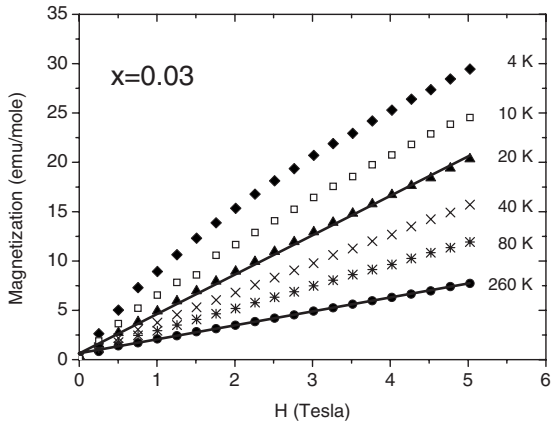

FIG. 6. Magnetization curves for the $x=0.03$ sample. The straight lines illustrate that the magnetization is a combination of the intrinsic component linear in H and an extrinsic superparamagnetic component that easily saturates to a value under the application of a small magnetic field. The straight lines have been drawn at 20 and 260 K only to improve clarity, but the same feature applies to all the magnetization curves in this range of temperatures. All these straight lines extrapolate at $H=0$ to the same magnetization (M_0 in the text), which is the magnetic extrinsic contribution of the ferromagnetic Fe nanoparticles at saturation.

This is no longer true at Fe concentrations $x=0.03$ since χ monotonically increases upon cooling. The concentration $x=0.03$ is then large enough so that the Fe-Fe magnetic exchange interaction becomes efficient. Note that there is about 1% Fe in $(2a)$ sites in this sample, after Table I, and this is found to break the singlet state, while the same amount of Fe on $(2d)$ sites in the $x=0.01$ sample could not do it. This is the first indication that Fe-Fe magnetic interactions are stronger in the basal planes. This will be confirmed in the next sections. Nevertheless, this iron concentration is yet too small to allow for a collective spin freezing of the Fe spins, at least in the range of temperatures ($T \geqslant 2$ K) investigated, hence the monotonous behavior of $\chi(T)$ and the absence of any difference between ZFC and FC measurements. The magnetization curve $M(H)$ of the $x=0.03$ sample is reported in Fig. 6. At $T<20$ K, the magnetization curves are no longer linear in H even at a large magnetic field, for reasons we have already discussed in a previous work on $Co_{1-x}Fe_xSb_3$.[2] On another hand, at $T \geqslant 20$ K, the magnetization curves $M(H)$ in Fig. 6 show that M can be decomposed in an extrinsic component that easily saturates under the application of the magnetic field, plus a linear-in-H intrinsic component. We have already observed this behavior in $Co_{1-x}Fe_xSb_3$ (Ref. 2) and argued that the extrinsic component is the superparamagnetic contribution of magnetic nanoparticles. Actually, at large enough magnetic field H so that the magnetization associated with the magnetic particles is saturated to a value M_0, we can write

$$M(H) = M_0 + \chi H, \tag{1}$$

where χ is the intrinsic magnetic susceptibility. M_0 can thus be easily determined by the linear extrapolation of the high-

field magnetization curve to $H=0$ and is temperature independent. Due to the high annealing temperature of the samples, the impurity phase in our material is more likely α-Fe. Since the magnetic moment carried by a Fe atom in α-Fe is $2.22\mu_B$, we find that the concentration of Fe that has precipitated under this form is 5.36×10^{-3} at. %, a concentration much too small to be detected by XRD. Since $x=0.03$, only a fraction $5.36\times10^{-3}/3$, i.e., 0.18%, of the iron has precipitated in this sample. Note, however, that we did not detect any α-Fe precipitate in our samples of larger compositions. This is another evidence that it is difficult to substitute Co by Fe at low concentrations of Fe. We have already shown that Fe occupies the $(2d)$ interstitial sites instead of the $(2a)$ Co sites when $x<0.03$. Now, we find that an increase of the Fe concentration up to $x=0.03$ is obtained at the price of the formation of α-Fe precipitates. Only at larger concentrations could we obtain samples with the total amount of iron inserted in the matrix in the $(2a)$ and $(2d)$ sites.

Results of the measurements of the magnetic susceptibility at larger Fe concentrations $X_{\mathrm{Fe}}>3$ at. % are illustrated in Fig. 7. χ^{-1} rather than χ has been plotted as a function of T in an attempt to fit the data with a Curie–Weiss law. However, the $\chi^{-1}(T)$ curves are nonlinear even at a high temperature up to $x=0.4$. Nevertheless, this is only due to the nonnegligible Pauli contribution since the data can be fit by a generalized Curie–Weiss law of the form

$$\chi(T)=\chi_0+\frac{C}{T-\theta}. \tag{2}$$

The fit is illustrated in Fig. 7. χ_0 is a positive constant that corresponds to the temperature-independent Pauli contribution of the electron gas. The values of θ determined by the fit are negative (antiferromagnetic coupling) and are in the range $|\theta|\leqslant 26K$ in the whole range of compositions $x\leqslant 0.5$. The effective moment μ defined by $C=x_{\mathrm{Fe}}\mu^2/(3k_B)$ is reported in Table I and found to be increasing with the Fe concentration.

B. Analysis

To make contact with prior works on other binary alloys crystallized in the so-called NiAs structure for which the conventional notation is NiAs rather than $Ni_{0.5}As_0.5$, we take the notation "CoSb" and $Fe_{1+\delta}Sb$ for our binary samples in this section only.

There are different models to describe magnetic properties associated with iron in solids, which correspond to different behaviors that have been observed. The strong d-d Coulomb correlations may in some cases generate a heavy fermion behavior like in $LaFe_4Sb_{12}$.[10] The Stoner model of band magnetism considers the case where both the electrons and the magnetic moments are delocalized like in α-Fe. The opposite model is the ionic model in which both the d electrons and the magnetic moments are assumed to be localized by the intra-atomic Coulomb correlations. An archetype of such an ionic compound is $LiFePO_4$.[11] Here, we show the intermediate case: both the c/a ratio and the existence of a Pauli contribution to the magnetic susceptibility show that the d electrons of iron are delocalized; on the other hand, the Curie–Weiss contribution to the magnetic susceptibility shows that the magnetic moments are localized. This is the situation seen in Heusler alloys[12] and in other iron compounds.[13] In the case of materials T_rX crystallizing in the NiAs structure, this behavior has been observed with $T_r=$Mn, and it has been understood from electronic structure calculations in MnAs and MnSb.[14,15] Although such calculations are missing for the particular material investigated here, the results can be extrapolated. First, the calculations have shown that the magnetic moment carried by the transition metal element is about the same whether it is calculated in a ferromagnetic or an antiferromagnetic alignment, which proves that it can be considered as localized.[16] This is in essence to the reason why the Curie–Weiss law applies at high temperature in our material. Second, the localized magnetic moment is small because the covalent bonding interaction between the $3d$ electrons of the transition element, whether direct or mediated by the $5p$ orbitals of Sb, leads to a lowering of the local magnetic moment.[16] In MnSb, for instance, the Mn atom is in configuration $3d^{5.5}$ with a localized magnetic moment of $3.3\mu_B$ only. Note that such a moment estimated from electronic structure calculations should not be confused with the effective moment we have deduced from the Curie–Weiss law. Due to the quenching of the orbital momentum, the moment of $3.3\mu_{\mathrm{B}}$ should behave like a pure effective spin $S=3.3/2=1.65$, which is confirmed by measurements that show that the gyromagnetic factor g is close to $g=2$.[17] Then, the corresponding effective magnetic moment deduced from the Curie law should be $\mu=2[S(S+1)]^{1/2}=4.18\mu_B$. The moment we found in Table I increases with the Fe concentration and saturates to a value $\simeq 3.7\mu_B$ that is smaller but comparable to that of Mn in MnSb and in both cases differ from the value of the moment predicted for Mn^{2+} or Fe^{3+} ions in ionic compounds. This is another evidence that the Fe-rich samples are metallic and the electronic configuration of iron should not be confused with that of Fe^{3+}. This may be the reason for an outstanding disagreement with the magnetic moment $\mu=0.88\mu_B$ estimated from the analysis of spin-polarized neutron experiments for Fe atoms of $(2a)$ sites[3] in $Fe_{1+\delta}Sb$, since the magnetic form factor of Fe^{3+} was used to fit the neutron spectra. In addition, such a small value of $\mu=0.88\mu_B$ would not be compatible with the antiferromagnetic (AF) ordering that is observed in $Fe_{1+\delta}Sb$ in the same work[3] because the loss of exchange energy resulting from the loss of local magnetization stabilizes the ferromagnetic alignment.[12]

The effective magnetic moment at small Fe concentrations is small. This is due to the fact that the proportion of Fe in $(2d)$ sites is larger, and the magnetic moment is expected to be smaller on the $(2d)$ Fe sites than that on $(2a)$ Fe sites. The reason is related to the metallic character of Fe-rich samples: the d electrons are itinerant mainly because of the d-d covalent interactions along the c axis,[9] and this covalent bonding along c is responsible for a lowering of the magnetic moment on the $(2d)$ Fe sites. The extreme case is again MnSb since it was concluded from neutron experiments that the Mn atoms in $(2d)$ sites have no magnetic moment.[18] In

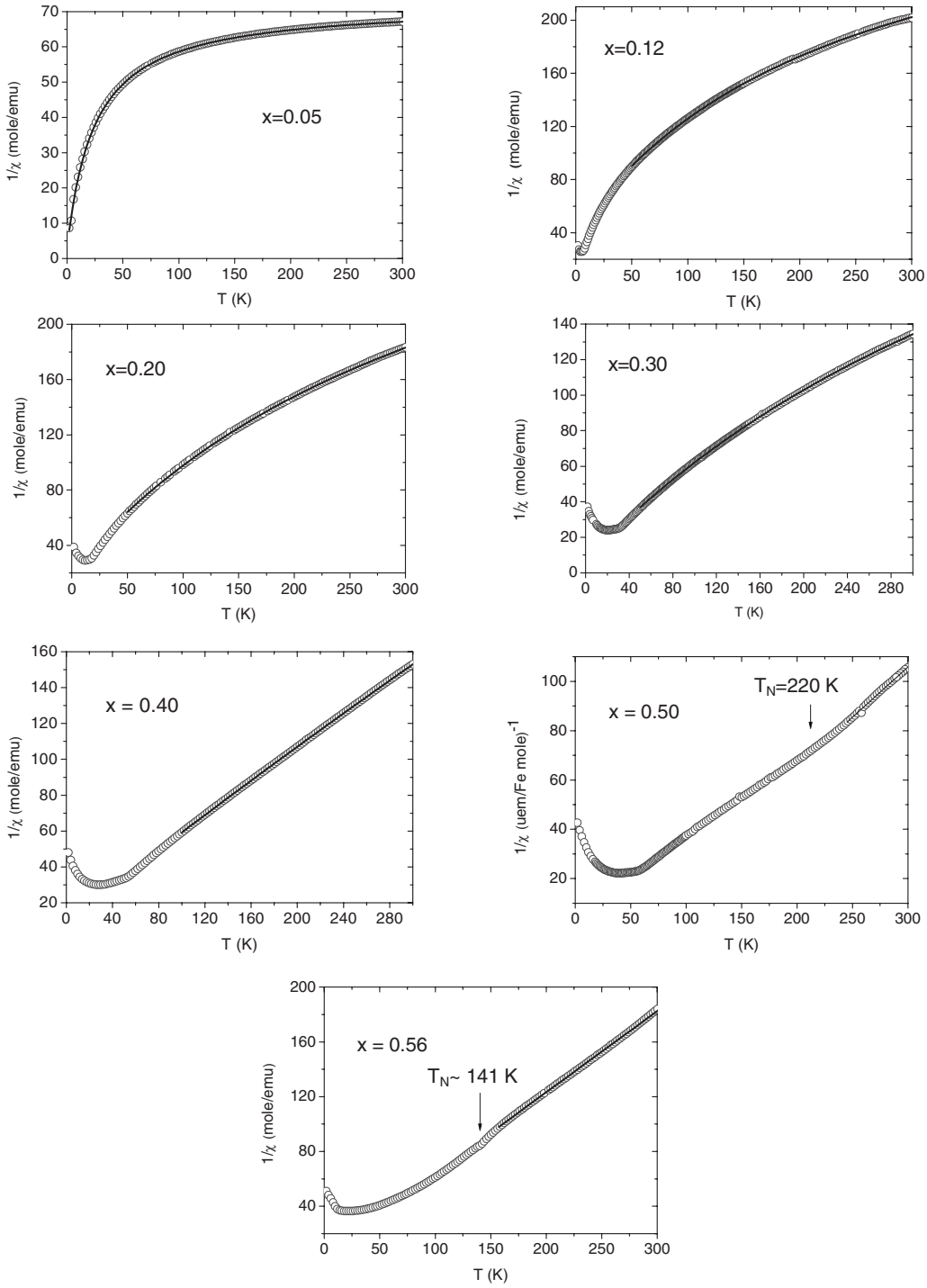

FIG. 7. Zero-field-cooled magnetic susceptibility $\chi(T)$ measured at dc magnetic field $H=0.1$ T for samples with Fe concentration $x>0.03$. The formula unit is $Co_yFe_xSb_z$ with $x+y+z=1$ according to Table I. The symbols are experimental values; the full lines are theoretical fits by the modified Curie–Weiss law.

the case of Fe, however, we have determined that Fe in $(2d)$ sites are magnetic with a magnetic moment that, however, is small according to Table I. The second difference between Mn and iron is the more metallic character of FeSb, which is evidenced by the larger $c/a=1.396$ ratio in MnSb, which means that the d-d interactions are larger in FeSb. Since they lower the center of mass of the occupied d band in the AF configuration but not in the ferromagnetic one, the $d-d$ interactions are known to favor antiferromagnetic alignment.[16] This is in essence to the reason why the magnetic ordering that is ferromagnetic in MnSb is antiferromagnetic in FeSb.

The difference in the local magnetic moment on $(2a)$ and $(2d)$ Fe sites implies that the value of the effective magnetic moments in Table I is actually an average of the square of the effective moments μ_{2a} and μ_{2d} on $(2a)$ and $(2d)$ Fe sites, respectively,

$$\mu^2 = f\mu_{2a}^2 + (1-f)\mu_{2d}^2, \quad (3)$$

where f is the fraction of Fe located on $(2a)$ sites displayed in Fig. 4. However, it is impossible to determine μ_{2a} and μ_{2d} from our experiments because these quantities depend on the ionic/covalent character of the bonds and thus depend on the Fe concentration. Local probes such as Mössbauer or neutron experiments are needed for that purpose.

V. MAGNETIC BEHAVIOR AT LOW TEMPERATURE

A. Antiferromagnetic ordering in Fe-rich samples

For the samples $x=0.5$ and 0.56, the inverse of the magnetic susceptibility shows an anomaly at $T_N \simeq 220$ and 141 K, respectively, marked by arrow in Fig. 7. This anomaly is much easier to detect on the $\chi^{-1}(T)$ curves like in Fig. 7 than that on $\chi(T)$ curves because it is superposed on an almost linear background. At such large Fe concentrations, the Pauli term χ_0 is too small with respect to the Curie–Weiss contribution to generate sizable deviations from the linearity of χ^{-1} vs T, so that this anomaly is entirely attributable to the transition to the antiferromagnetic order. We believe that this is the reason why no anomaly at T_N could be detected in a prior work where $\chi(T)$ instead of $\chi^{-1}(T)$ was explored.[19] No difference between ZFC and FC curves can be observed in the vicinity of T_N, so that T_N can be identified with a Néel temperature. This result is consistent with the prior work in Ref. [3] The decrease of T_N with δ (Ref. 4) quantitatively accounts for the shift from $T_N=105$ K in Ref. 3 to $T_N=141$ K in our $x=0.56$ sample. On the another hand, the fact that the anomaly at T_N is so small gives evidence that only part of the spins is frozen in an AF configuration. Two hypotheses can be invoked. The first hypothesis is that the magnetic transition at T_N corresponds to the formation of three-dimensional antiferromagnetic clusters of finite size, in which case the Fe interstitials also order at T_N.[4] The other hypothesis is that only the normal Fe atoms on $(2a)$ sites order at T_N.[3] The magnetic properties we have investigated only give access to macroscopic properties and do not allow us to conclude which one out of these two hypotheses is the right answer. Nevertheless, our results give some insight on the different roles played by Fe atoms on the two different sites.

To investigate these roles, let us first consider the magnetic interactions between the different iron atoms. The magnetic interaction between an iron ion in the $(2a)$ site and a nearest neighbor on the $(2d)$ site, when it is occupied, is expected to be essentially a direct interaction according to the Moriya mechanism[20] just like the interaction J_1 between $(2a)$ nearest neighbors along the c axis and, thus, positive (ferromagnetic). The reason is that the distance between such atoms is smaller than a (it is only $c/2 \simeq 0.26$ Å for J_1), so that this direct exchange interaction that is ferromagnetic is much larger than the superexchange interaction that is antiferromagnetic. Then, the increase in the population of the $(2d)$ sites just increases the number of ferromagnetic bonds between Fe atoms that opposes the antiferromagnetic ordering. This feature explains the decrease of T_N with δ that has been observed in $Fe_{1+\delta}Sb$.[4] On the other hand, the distance between nearest $(2a)$ sites is a, which is large enough so that the antiferromagnetic superexchange interactions are dominant, which explains the triangular spin arrangement of Fe magnetic moments in the basal plane at T_N, evidenced by neutron experiments.[3] This, in essence, explains the magnetic behavior of the $x=0.56$ sample. To understand Fe spin dilution effects, we note that the concentration of $(2d)$ interstitial sites occupied by Fe in the $x=0.50$ and $x=0.56$ samples is the same, so that any difference in their magnetic properties only comes from the vanishing of the substitution of Co atoms by Fe atoms in the $(2a)$ sites (see Table I) in the $x=0.50$ sample with respect to 6% in the $x=0.56$ sample. It results in an increase in T_N that reaches $T_N \simeq 220$ K in the $x=0.50$ sample, despite the dilution of Fe magnetic moments upon substitution of magnetic Fe by nonmagnetic Co in the $(2a)$ sites of the hexagonal lattice in the basal planes. The reason is the decrease of a that increases the strength of the antiferromagnetic coupling inside the basal plane.

The relative concentration r of Fe with respect to Co in the basal planes shifts only from $r=100\%$ in the $x=0.56$ sample to $r=38/44=86\%$ in the $x=0.50$ sample, so that it remains large with respect to the percolation threshold r_c for the basal magnetic lattice. The decrease in T_N versus r is small near $r=1$ and strong only as one approaches the percolation threshold, which is the reason why the variation of T_N between the two samples is dominated by the other effect mentioned above. On the other hand, the spin dilution effects did not allow this collective antiferromagnetic ordering in our samples $x \leqslant 0.40$. Indeed, the site percolation threshold of the two-dimensional (2D) triangular lattice is 0.5. The occupation number of the lattice sites in the basal planes by Fe atoms for the $x=0.30$ sample is $r=22/46$ below the percolation threshold. On the other hand, r is already larger than 0.5 for $x=0.40$ and the S-shaped form of the magnetization curve, which is characteristic of the re-entrance at low temperature, as we shall see in the next section, also pleads for an antiferromagnetic transition at finite temperature. We cannot exclude that this transition exists even if we could not detect it since we have already pointed out the difficulty to detect it even in the $x=0.56$ sample. We must also remember that the existence of geometric frustration associated with the existence of antiferromagnetic interactions may be responsible for the disappearance of T_N at a value of r larger than the site percolation. In any case, the fact that the limit in the apparition of the antiferromagnetic ordering is comparable to the site percolation of the 2D lattice comforts the hypothesis that only the Fe spins in $(2a)$ sites in the basal plane order at T_N that is in agreement with neutron experiments,[3] although a different conclusion was derived from Mössbauer analysis.[4] It also gives evidence that the magnetic interactions are short range and thus dominated by direct Fe-Fe exchange and superexchange interactions.

B. Spin-glass and re-entrant spin-glass transitions

All the samples $x \geqslant 0.12$ show similar magnetic properties at low temperature. The departure between FC and ZFC $\chi(T)$ curves takes place at temperature T_2. Upon cooling below T_2, a sharp separation between FC and ZFC $\chi(T)$ curves takes

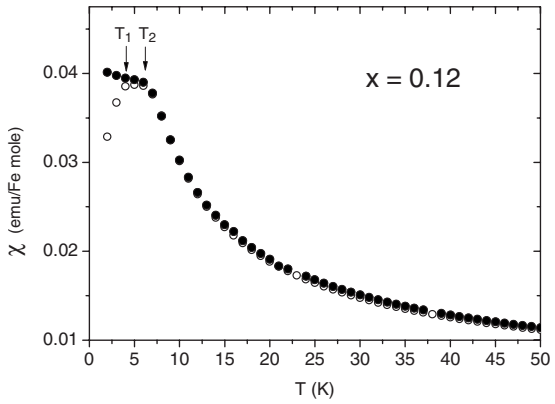

FIG. 8. Zero-field-cooled (open circles) and field-cooled (full circles) magnetic susceptibilities $\chi(T)$ measured at a dc magnetic field of 0.1 T for the $x=0.12$ sample.

place at a temperature we call T_1, at which the ZFC curve goes through a maximum, while the FC curve still increases upon cooling. These features are shown in Figs. 8 and 9 for the $x=0.12$ and $x=0.4$ samples, which are chosen as examples.

At high concentrations $x \geqslant 0.4$, the low field part of the magnetization curves presents an inverse curvature and an inflection point, as can be seen in Fig. 10. This feature is a characteristic of re-entrant spin-glass phases of either ferro- or antiferromagnets.[21] The change of behavior from pure antiferromagnet [linear $M(H)$] to a re-entrant spin-glass phase [S-shaped $M(H)$] is also used to distinguish between these two phases in other frustrated compounds.[22] The Fe concentration in the $x=0.40$ sample is a limit case where we could not detect any temperature T_N for AF ordering, while we still observe this S-shape $M(H)$ curve.

Note that the transitions at T_1 and T_2 are observed in samples $x>0.4$ that order antiferromagnetically at larger temperature T_N, in which case T_1 and T_2 correspond to re-entrant spin-glass phases. However, they are also observed in those samples $x<0.4$ that do not show any AF ordering, in which case T_1 and T_2 correspond to spin-glass phases. This is understandable because spin-glass and re-entrant spin-glass phases are two irreversibility levels that present the same features and are phase transitions with the same dynamics.

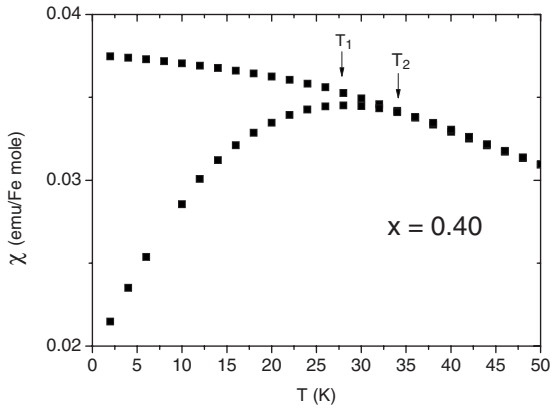

FIG. 9. Same as Fig. 8 for the $x=0.4$ sample.

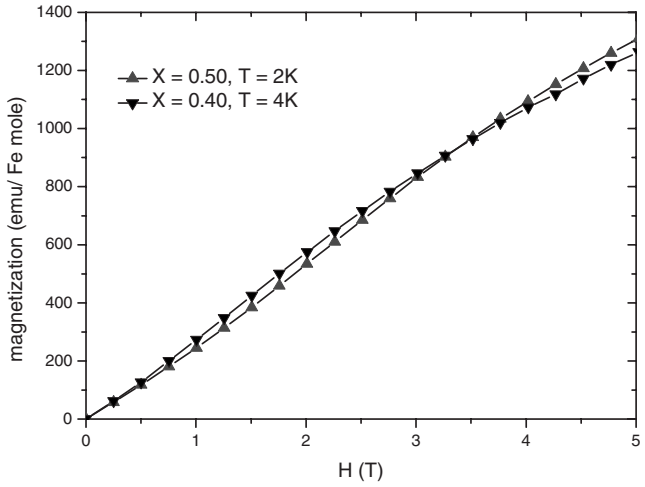

FIG. 10. Magnetization curves of the $x=0.4$ and $x=0.5$ samples at low temperature.

The variations in T_1, T_2, and T_N as a function of x are reported in Fig. 11. However, it is important to realize that these temperatures depend on the relative amount f of Fe atoms on $(2a)$ sites. A true magnetic phase diagram of the material would then be the three-dimensional plot of these temperatures in the space (T,x,f). The dependence on f, however, has been determined only in $Fe_{1+\delta}$ so far.

To complete the study of spin freezing at T_2, we have measured the ac magnetic susceptibility at different frequencies in the range of $0.1 \leqslant \nu \leqslant 800$ Hz. The result is illustrated in Fig. 12 for the $x=0.12$ sample. The onset of irreversibility takes place at a temperature T_f larger than the temperature

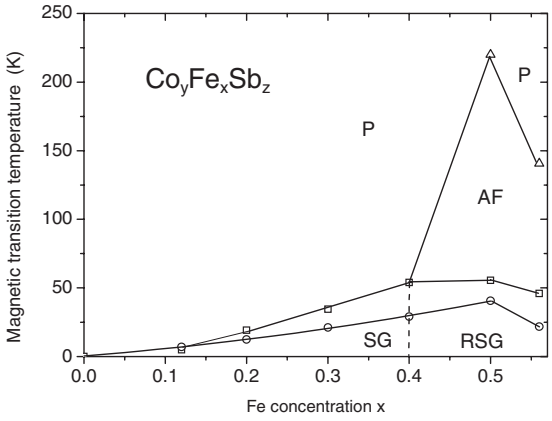

FIG. 11. Magnetic phase diagram of the CoSb-$SbFe_{1+\delta}$ system. P stands for the paramagnetic phase, SG for the spin-glass phase, RSG for the re-entrant spin-glass phase, and AF for the antiferromagnetic phase. Note that this diagram depends on the amount of Fe on $(2d)$ interstitial sites. The symbols are data obtained on the samples detailed in Table I. Open triangles are Néel temperatures, open squares denote T_2, and open circles denote T_1. The lines are guides for the eyes. In particular, the line that delimitates the antiferromagnetic ordering should not look like a triangle and should be refined by additional data on samples in the range of $0.4<x<0.56$, which would give a more rounded curve ending by a more vertical slope as one approaches the percolation limit in the vicinity of $x=0.4$ (see in the text).

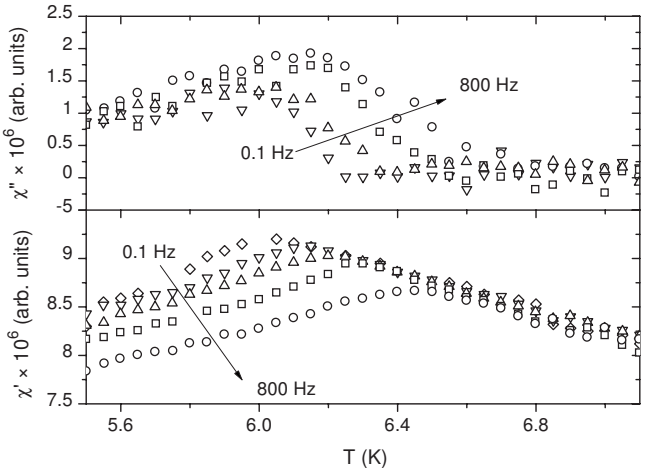

FIG. 12. Real (χ') and imaginary (χ'') parts of the magnetic susceptibility at an ac field of 3 Oe at frequencies of 0.1, 1, 10, 100, and 800 Hz for the $x=0.12$ sample.

T_{max} of the maximum in the ZFC-$\chi'(T)$ curve. Note that T_f and T_{max} differ from T_2 and T_1, respectively, not only because the quantities have been measured at different time scale but also because the amplitude of the magnetic field is different (an ac magnetic field of 0.3 mT, against a dc field of 0.1 T). In this work, however, the influence of the strength of the magnetic field on the dynamics was not explored, and no dc magnetic field was superposed to the ac field. T_{max} is often used for the definition of the spin-glass or re-entrant spin-glass transition. However, we have argued that this maximum does not have any clear physical meaning and we shall retain T_f as the transition temperature.[23] Note that T_f also coincides with the departure of $\chi\prime\prime(T)$ from zero. T_f considerably shifts to a lower temperature with decreasing frequency like in canonical spin glasses. An attempt at fitting the $T_f(\nu)$ to the Vogel–Fulcher scaling law,

$$\ln\left(\frac{\nu}{\nu_0}\right) = -\frac{E_a}{k_B(T_f - T_0)}, \tag{4}$$

gives $T_0=5.6$ K, $E_a=2.8\times10^{-22}$ J, and $\tau_0=\nu_0^{-1}=3.7\times10^{-12}$ s for the $x=0.12$ sample, while the analysis in terms of the conventional critical slowing down for spin glasses,

$$\left(\frac{\nu}{\nu_0}\right) = \left(\frac{T_f - T_0}{T_0}\right)^{z\nu}, \tag{5}$$

gives $T_0=6.1$ K, and the dynamic critical exponent $z\nu=9.6$. These values for both $z\nu$ and τ_0 are typical values in conventional spin glasses.[24] In particular, we find that τ_0 is the characteristic time of atomic spin flipping, which is the evidence that the magnetic phase transition is indeed the spin-glass or re-entrant spin-glass freezing. It precludes the possibility of a cluster glass, i.e., a freezing of magnetic clusters, since the time τ_0 would have been the characteristic time associated with the flipping of the polarization of one cluster, which is orders of magnitude larger than the atomic relaxation time. These features are the same at any concentration; only the temperatures T_f and T_0 depend on x (and increase with x). The difference in T_0 in the two fits by Eqs. (4) and (5) is also commonly observed in any spin glass and has been discussed elsewhere.[25]

$\chi''(T)$ goes through a maximum at a temperature T_i slightly smaller than T_f. This maximum in $\chi''(T)$ also corresponds to an inflection point in the ZFC-$\chi'(T)$ curve. This feature corresponds in some cases to the signature of the transition to a re-entrant phase.[26] In the present case, however, this is only a secondary maximum because the sharp increase in the difference between the ZFC and FC magnetic susceptibilities at a temperature that is T_1 when $H=0.1$ T in quasistatic conditions implies that the main peak in $\chi''(T)$ will be near T_1. Therefore, the secondary maximum of $\chi''(T)$ at T_i, here, might just be the result of sample inhomogeneities that would spread the transition at T_f, with the onset of magnetic irreversibility extending from T_f to T_i. Indeed, the frequency dependences of T_f and T_i are just the same, so that they are associated with the same physical process, while T_1 corresponds to a transition to another spin-glass state.

VI. DISCUSSION

The existence of two (re-entrant or not) spin-glass phases has been observed in several cases and is predicted by the model of Gabay–Toulouse.[27] According to this model, T_2 would correspond to the onset of spin-glass ordering of the transverse components of the spins, while T_1 would be associated with the additional freezing of the longitudinal component of the spins. Since this freezing of the longitudinal component transition is also associated with the breaking of the replica symmetry, it is associated with the onset of strong magnetic irreversibility at T_1. In case the AF ordering at T_N is observed ($x>0.4$), the magnetic phases below T_2 are re-entrant spin-glass phases in which both the antiferromagnetic order and the spin-glass phase coexist.

The results are comparable to the magnetic properties of $Ni_cMg_{1-c}(OH)_2$ at large Ni concentrations ($c>0.6$), which is another diluted antiferromagnet. This material crystallizes in the CdI_2 type, which is also a hexagonal structure, in which the magnetic ions (Ni^{2+}) form a triangular lattice. At large c, the system also antiferromagnetically orders (although the type of AF order is different), and the magnetic susceptibility curves show the same features,[28] namely, the onset of magnetic irreversibility at some temperature below T_N [the analog of the temperature T_2 in the present work, but no attention was paid to this feature in this prior work on $Ni_cMg_{1-c}(OH)_2$] and a dramatic increase of irreversibility at temperature T_1 that coincides with a peak in $\chi''(T)$ referred as the transition temperature to the re-entrant spin-glass phase. The difference between the two systems is in the magnetic behavior in more dilute systems. For instance, at $c=0.5$, the peaks in the $\chi'(T)$ and $\chi''(T)$ curves are almost frequency independent, while in typical spin glasses, including the system Co-Sb-Te investigated here, these peaks shift to higher temperature with increasing frequency of the ac magnetic field.[29] This anomalous behavior in $Ni_cMg_{1-c}(OH)_2$ is also observed in Fe_cMgCl_2 at similar dilutions $c\simeq0.5$.[30] The common feature of the two systems is that they are diluted Ising antiferromagnets, the Ising character in the case of $Ni_cMg_{1-c}(OH)_2$ coming from the chiral-

ity of spin triads, and the universality class of the chiral-glass transition is that of the three-dimensional Ising spin glass.[31] The different spin dynamics that we observe in our system can then be considered as an evidence that it does not belong to the Ising family, so that the magnetic anisotropy should be small in our material. This is confirmed by the complex AF order in our system with magnetic moments polarized in different directions in the basal plane,[3] while the Fe spins are aligned along the c axis by the Ising anisotropy in $FeMgCl_2$.

The coexistence of the spin-glass and antiferromagnetic orders in the re-entrant spin-glass phase has been previously observed on other systems.[32,33] We believe that this is the reason why the magnetic structure observed by the neutron experiments is still retained below 28 K in $Fe_{1+\delta}Sb$.[3] In the same way, the neutron experiments have shown that the AF order is not affected by the re-entrant spin-glass transition in $Fe_cMg_{1-c}Cl_2$ at $c=0.55$.[30] The re-entrance phenomena in $Fe_{1+\delta}Sb$ comes from the excess Fe on the $(2d)$ sites that introduce an inhomogeneity in the distribution of the magnetic interactions. Actually, the theoretical models for spin glass and re-entrant spin glasses separate in two main classes: the homogeneous models[27] and inhomogeneous models.[34] In a homogeneous picture, the coexistence of long-range AF and spin-glass orders takes place everywhere simultaneously in the material. In a homogeneous picture, the system is divided in regions where either AF or spin glass dominates. Since both approaches give similar phase diagrams, it is usually quite difficult to distinguish between these two possibilities, but the re-entrance we have observed even in the absence of spin dilution in the basal planes pleads in favor of the inhomogeneous case in our system.

VII. CONCLUSION

The ternary compounds relating CoSb to $Fe_{1+\delta}$ have been synthesized. They all crystallize in the NiAs structure. The XRD analysis, however, gives evidence of the difficulty to substitute Co by Fe in the basal planes with a tendency for Fe to occupy interstitial $(2d)$ sites in the low Fe-concentration limit. The fraction f of Fe on $(2a)$ sites increases with the total amount x of Fe atoms. The static and dynamic magnetic properties have been investigated. The effective moment associated with the d electrons remains localized on the Fe sites despite the metallic character, a feature that is met in other transition compounds crystallizing in this NiAs structure. The magnetic moment of Fe on $(2d)$ sites is smaller than that on $(2a)$ sites but does not vanish like that of Mn on the same sites in MnSb. At $x>0.01$, the material behaves like a diluted antiferromagnet with small Ising anisotropy. The antiferromagnetic long-range ordering is observed for Fe concentrations in the basal plane that exceed the site percolation threshold for the triangular lattice, which is consistent with the results of neutron experiments showing that only the magnetic moment of Fe on $(2a)$ sites order at T_N in $Fe_{1+\delta}Sb$. At low temperatures, the system undergoes magnetic transitions to spin-glass phases with critical slowing down and relaxation times that are consistent with the values met in conventional spin glasses. These phases coexist with the AF order at large Fe concentrations. Although an overall understanding of the magnetic properties has been achieved, further magnetic neutron-scattering studies are required to provide us with an independent determination of the magnetic moment carried by Fe on $(2a)$ sites since the former analysis of the magnetic intensities in neutron studies have been analyzed by assuming a configuration Fe^{3+} that is not relevant to Fe in these materials.

ACKNOWLEDGMENT

Institutes 1 and 2 are associated with Centre National de la Recherche Scientifique.

*Laboratoire associé au Centre National de la Recherche Scientifique.

[1] J. W. Allen and W. Stutius, Solid State Commun. **20**, 561 (1976).
[2] P. Amornpitoksuk, D. Ravot, A. Mauger, and J. C. Tedenac, J. Alloys Compd. **440**, 295 (2007).
[3] T. Yashiro, Y. Yamaguchi, S. Tomiyoshi, N. Kazama, and H. Watanabe, J. Phys. Soc. Jpn. **34**, 58 (1973).
[4] R. Kumar, K. S. Harchand, Vishwamittar, K. Chandra, P. Jernberg, T. Ericsson, and R. Wäppling, Phys. Rev. B **32**, 69 (1985).
[5] J. Nösselt and U. Sondermann, Int. J. Magn. **5**, 277 (1973).
[6] P. J. Picone and P. E. Clark, J. Magn. Magn. Mater. **25**, 140 (1981).
[7] K. Ishida and T. Nishizawa, *Binary Alloy Phase Diagrams* (American Society for Metals, Metals Park, OH, 1990), p. 1232.
[8] H. Okamoto, *Binary Alloy Phase Diagrams* (American Society for Metals, Metals Park, OH, 1990), p. 1763.
[9] A. Kjekshus and W. B. Person, Prog. Solid State Chem. **1**, 83 (1964).
[10] R. Viennois, S. Charar, D. Ravot, P. Haen, A. Mauger, A. Bentin, S. Paschen, and F. Steglich, Eur. Phys. J. B **46**, 257 (2005).
[11] K. Zaghib, A. Mauger, J. B. Goodenough, F. Gendron, and C. M. Julien, Chem. Mater. **19**, 3740 (2007).
[12] J. Kübler, A. R. Williams, and C. B. Sommers, Phys. Rev. B **28**, 1745 (1983).
[13] R. Viennois, D. Ravot, J. C. Tedenac, S. Charar, and A. Mauger, Mater. Sci. Eng., B **119**, 1 (2005).
[14] L. M. Sandratskii, R. F. Egorov, and A. A. Berdyshev, Phys. Status Solidi B **103**, 511 (1981).
[15] R. Podloucky, Solid State Commun. **50**, 763 (1984).
[16] R. Coehoorn, C. Haas, and R. A. de Groot, Phys. Rev. B **31**, 1980 (1985).
[17] G. G. Scott, Phys. Rev. **121**, 104 (1961).
[18] Y. Yamagushi, H. Watanabe, and T. Suzuki, J. Phys. Soc. Jpn. **41**, 703 (1976).
[19] K. Yamagushi, H. Yamamoto, Y. Yamagushi, and H. Watanabe, J. Phys. Soc. Jpn. **33**, 1292 (1972).
[20] T. Moriya, Prog. Theor. Phys. **33**, 157 (1965).
[21] H. Aruga Katori, T. Goto, S. Ebii, and I. Ito, J. Magn. Magn. Mater. **104-107**, 1639 (1992).
[22] T. H. Kim, M. C. Cadeville, A. Dinia, and V. Pierron-Bohnes,

and H. Rakoto, Phys. Rev. B **54**, 3408 (1996).
[23] A. Mauger, J. Ferré, M. Ayadi, and P. Nordblad, Phys. Rev. B **37**, 9022 (1988).
[24] S. Galam and A. Mauger, J. Phys. I **4**, 467 (1994).
[25] N. Bontemps, J. Ferré, and A. Mauger, J. Phys. (Paris), Colloq. **8**, 1063 (1989).
[26] M. Escorne, M. Godinho, J. Tholence, and A. Mauger, J. Appl. Phys. **57**, 3424 (1985).
[27] M. Gabay and G. Toulouse, Phys. Rev. Lett. **47**, 201 (1981).
[28] M. Suzuki, I. Suzuki, and T. Enoki, J. Phys.: Condens. Matter **12**, 1377 (2000).
[29] J. A. Mydosh, *Spin Glasses: An Experimental Introduction* (Taylor & Francis, London, 1993).
[30] P. Z. Wong, S. von Molnar, T. T. M. Palstra, J. A. Mydosh, H. Yoshizawa, S. M. Shapiro, and A. Ito, Phys. Rev. Lett. **55**, 2043 (1985).
[31] H. Kawamura, Int. J. Mod. Phys. C **7**, 345 (1996).
[32] K. Binder and A. P. Young, Rev. Mod. Phys. **58**, 801 (1986).
[33] S. M. Shapiro, G. Aeppli, H. Maletta, and K. Motoya, Physica B **137B**, 96 (1986).
[34] H. Takayama, J. Phys. Soc. Jpn. **61**, 2512 (1992).